Study of Atmospheric Effects on Satellite Synthetic Aperture Radar (SAR) Measurements in Tropical Regions

Z.W. LI, X.L. DING, G.X. LIU, Y.Q. CHEN, Z.L. LI and J.J. ZHU, China

Key words: SAR, InSAR, GPS, atmospheric delays, tropospheric zenith delays (ZNDs).

ABSTRACT

Repeat-pass interferometric synthetic aperture radar (InSAR) has been demonstrated to be very useful for topographic mapping and surface deformation measurement. However, satellite synthetic aperture radar (SAR) data are often seriously contaminated by atmospheric delays of the radar signals. Due to the highly variable nature of the atmosphere, especially the atmospheric water vapor, it is often difficult to accurately model and correct the atmospheric effects. Consequently, significant errors can potentially be resulted in InSAR measurements, especially in tropical regions like Hong Kong.

Atmospheric effects on InSAR measurements in the Hong Kong region are studied based on a tandem pair of InSAR data and a month-long continuous GPS (CGPS) tracking data obtained at six stations. Differential atmospheric signals extracted from the SAR data for two selected areas in Hong Kong show apparent power law nature of the signals. The RMS values of the signals are 2.12 and 3.40 rad respectively for the two areas. The GPS tropospheric zenith delays (ZNDs) estimated indicate that a peak-to-peak error of about 9.36 cm can potentially be resulted in a SAR interferogram at the 95% significance level even with only a one-day interval. The error increases to about 11.47 cm for a ten-day interval.

CONTACT

Dr. X.L. Ding
Department of Land Surveying and Geo-Informatics
The Hong Kong Polytechnic University
Hung Hom, Kowloon
HONG KONG, CHINA
Tel. + 852 2766 5965
Fax + 852 2330 2994
E-mail: lsxlding@polyu.edu.hk
Web site: http://www.polyu.edu.hk

Study of Atmospheric Effects on Satellite Synthetic Aperture Radar (SAR) Measurements in Tropical Regions

Z.W. LI, X.L. DING, G.X. LIU, Y.Q. CHEN, Z.L. LI and J.J. ZHU, China

1. INTRODUCTION

Interferometric synthetic aperture radar (InSAR) has been applied widely in recent years. Its all-weather, day and night imaging capabilities, and unprecedented spatial coverage and resolution make it a unique technology for topographic mapping and ground displacement monitoring. InSAR has however some weakness. One of the most intractable problems is the atmospheric effect, especially the atmospheric water vapor, on repeat-pass SAR data (e.g., Massonnet and Feijl, 1995; Rosen et al., 1996; Tarayre et al., 1996; Zebker et al., 1997). Due to the highly variable nature of the atmosphere, it is difficult to accurately model and correct the atmospheric effects (Rosen, et al., 1999), especially in tropical regions like Hong Kong (HK).

This paper aims to assess the level of atmospheric effects on InSAR measurements in regions like HK based on both InSAR and GPS data. The principles of repeat-pass InSAR will be briefly outlined first. The processing of the SAR and GPS data will then be introduced and the results are analyzed.

2. REPEAT-PASS INSAR

The geometrical configuration of repeat-pass SAR interferometry is illustrated in Figure 1. A1 and A2 are positions of the radar platform corresponding to the two acquisitions. The phases, ψ_1 and ψ_2, measured at the two platform positions to a ground point are:

$$\psi_1 = \frac{4\pi}{\lambda}\rho_1, \qquad \psi_2 = \frac{4\pi}{\lambda}\rho_2 \tag{1}$$

where ρ_1 and ρ_2 are the slant ranges and λ is the radar wavelength. The interferometric phase ϕ is then

$$\phi = \psi_1 - \psi_2 = \frac{4\pi}{\lambda}(\rho_1 - \rho_2) \tag{2}$$

Under the far field approximation, we get

$$\phi = \psi_1 - \psi_2 \approx \frac{4\pi}{\lambda} B^{\parallel} = \frac{4\pi}{\lambda} B \sin(\theta - \alpha) \tag{3}$$

where α is the orientation angle of the baseline and θ is the look angle.
When assuming a surface without topographic relief as illustrated in Figure 2, the interferometric phase becomes (Rosen et al.1996)

$$\phi_0 = \frac{4\pi}{\lambda} B \sin(\theta_0 - \alpha) \tag{4}$$

where θ_0 is the look angle. If topography is present, the look angle will differ from θ_0 by $\delta\theta$

$$\phi = \frac{4\pi}{\lambda} B \sin(\theta_0 + \delta\theta - \alpha) \tag{5}$$

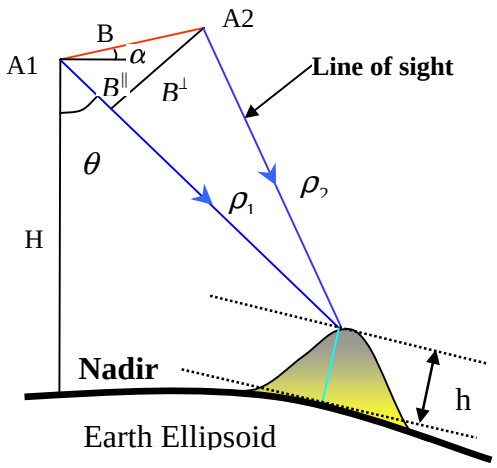

Figure 1. Interferometric geometry

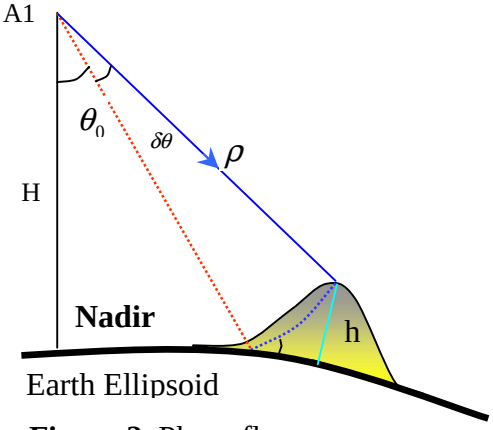

Figure 2. Phase flatten geometry

Combining equations (4) and (5), we get the "flattened" phase

$$\phi_{flat} = \phi - \phi_0 \approx \frac{4\pi}{\lambda} B \cos(\theta_0 - \alpha)\delta\theta = \frac{4\pi}{\lambda} B^{\perp}\delta\theta \tag{6}$$

Thus the topographic height can be expressed as

$$h \approx \rho\delta\theta \cdot \sin\theta_0 = \frac{\lambda}{4\pi B^{\perp}} \rho \sin\theta_0 \phi_{flat} \tag{7}.$$

If there exists a ground deformation Δr along the direction of radar line-of-sight (LOS) between the two SAR acquisitions, it will manifest itself in the phase difference (Rosen et al., 1996):

$$\phi_{flat} = \phi - \phi_0 \approx \frac{4\pi}{\lambda} \frac{B^{\perp}}{\rho \sin\theta} h + \frac{4\pi}{\lambda} \Delta r \tag{8}.$$

3. ATMOSPHERIC EFFECTS ON REPEAT-PASS INSAR

3.1 The atmosphere and its effect on repeat-pass InSAR

Among all the atmospheric layers, the ionosphere and the troposphere have the most effects on SAR radar signals. The ionosphere is dispersive whilst the troposphere is not. The troposphere contains about 80% of the total molecular mass of the atmosphere and nearly all the water vapor. The water vapor is a highly variable component in the troposphere and significantly affects SAR radar signals.

Two types of errors may potentially be introduced when microwave propagates through the atmosphere, the bending and the propagation delays. The latter dominates in case of InSAR measurements (Rosen et al. 1999). When taking into consideration of the propagation delay errors in InSAR, the phase measurements become,

$$\psi_1 = \frac{4\pi}{\lambda}(\rho_1 + \Delta\rho_1), \qquad \psi_2 = \frac{4\pi}{\lambda}(\rho_2 + \Delta\rho_2) \tag{9}$$

The interferometric phase then is

$$\phi = \psi_1 - \psi_2 = \frac{4\pi}{\lambda}(\rho_1 - \rho_2) + \frac{4\pi}{\lambda}(\Delta\rho_1 - \Delta\rho_2) \qquad (10)$$

where $\frac{4\pi}{\lambda}(\rho_1 - \rho_2)$ is the contributions from the topography and the surface deformation and $\frac{4\pi}{\lambda}(\Delta\rho_1 - \Delta\rho_2)$ is the contributions from atmospheric delays. It is easy to see that the latter will disappear if the atmosphere along the paths of the radar signals remains the same at the two acquisitions. The atmosphere however rarely remains unchanged between radar acquisitions. The atmospheric effects can be in this case easily interpreted as topography or surface deformations (Hanssen, 1998; Hanssen et al., 1999).

3.2 Atmospheric effects on InSAR measurements estimated from InSAR data

A SAR interferogram generated by complex conjugate multiplication of two SAR images is a superposition of information on topography height, surface deformations, differential atmospheric propagation delays between the acquisitions, and the noise (Tarayre et al., 1996; Hanssen, et al., 1999). If there is no surface deformation between the two image acquisitions or if the deformation is known, the atmospheric signatures can be extracted from an interferogram by eliminating the contribution of the topography.

An ESA ERS Tandem pair acquired on March 18 and March 19, 1996 over HK is used for this purpose. The perpendicular and parallel baseline components for the pair of images are 100 m and 78 m respectively. As the images have only a time interval of one day, it can be safely assumed that there is no surface deformation in the area between the SAR image acquisitions. Since satellite orbit errors generate in an interferogram phase shifts similar to those generated by long wavelength atmospheric disturbances (Tarayre, et al., 1996; Hanssen, 1998), careful baseline refinement is necessary in the interferometric processing. Figure 3

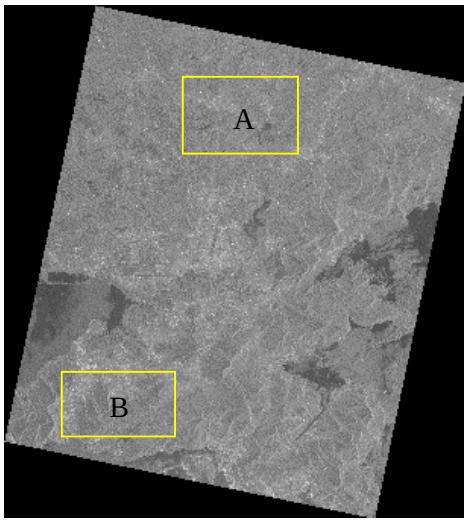

Figure 3. Amplitude SAR image of HK. A and B are a flat and hilly area, respectively, chosen for the study.

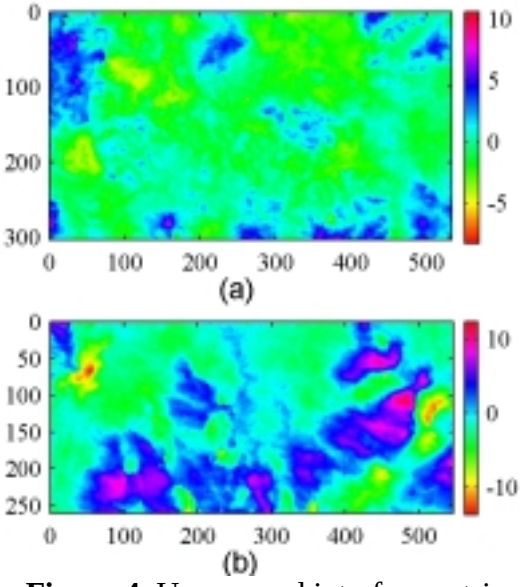

Figure 4. Unwrapped interferometric phases for areas A and B (with topographic phase removed)

shows one of the amplitude images, where rectangles A and B are a flat and a hilly areas respectively chosen for the study. The two areas are about 6km x 11km and 5km x 11km respectively in size.

For area A, since the perpendicular baseline is not too large (100 m as mentioned earlier) and the majority of the surface varies less than 10 m except for a small ridges with a height of less than 40 m in the northwest part, the variations of the interferometric phase can be considered due largely to radar signal path delays caused by the atmosphere (Hanssen, 1998). For area B, a DEM with an accuracy of better than 10 m from the Lands Department of the HK Government was used to remove the topographic component from the interferogram. Figure 4 shows the unwrapped interferometric phases in the two areas. The mean differential atmospheric delays in each of the areas are then calculated and removed from the results. A 2D Fast Fourier Transform (FFT) is performed next for each of the areas and the results are squared to obtain the power spectrums. The histograms and 1D rotationally averaged power spectrums thus obtained are given in Figures 5 and 6, respectively. The RMS of the differential atmospheric delays for the two areas are 2.12 and 3.40 rad, respectively.

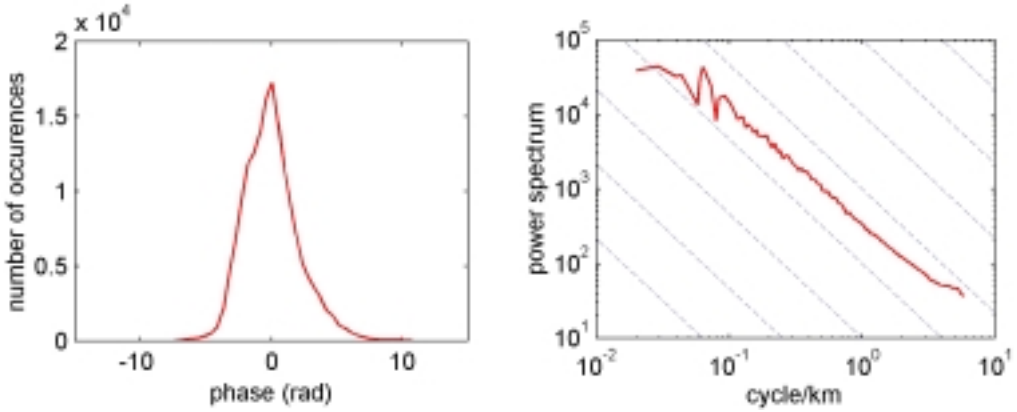

Figure 5. Histogram (left) and power spectrum (right) of differential atmospheric delays for area A

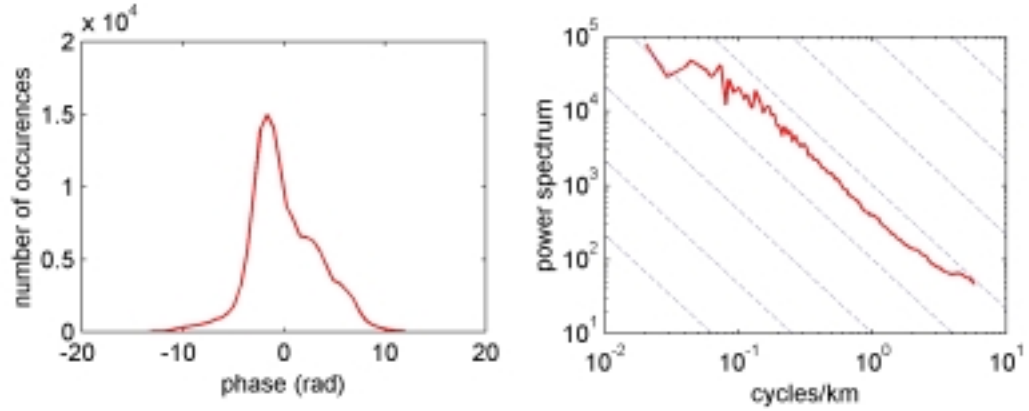

Figure 6. Histogram (left) and power spectrum (right) of differential atmospheric delays for area B

It is clear that the differential atmospheric delays in both of the areas on the whole follow the power law. The results are in good agreement with those presented by Hanssen (1998). The

dashed lines in the diagrams are the $-5/3$ power law values. The power law index varies with the scales slightly, which is consistent with the turbulence behavior of such phenomena as integrated water vapor (Christopher et al., 1997), and the wet delays in radio ranging.

3.3 Estimation of tropospheric delays from GPS measurements

Tropospheric zenith delays (ZNDs) can be resolved from high-accuracy GPS measurements along with other geodetic parameters such as the station coordinates (Bevis et al., 1992). The accuracy of ZNDs estimated from GPS measurements is generally around 6-8 mm (Bock and Williams, 1997). Since the troposphere is a non-dispersive medium, the ZNDs estimated from GPS measurements can be used to assess the tropospheric delays caused to SAR data with the assistance of a mapping function to convert the results into the direction of radar LOS.

There are currently six continuous GPS tracking stations covering the northwest regions of HK, which are Fanling, Kam Tin, Kau Yi Chau, Lam Tei, Siu Lang Shui and Shatin. The stations all started operations in 2000 or earlier. In this study, the GPS data collected in the whole month of March 2001 are used to estimate the hourly ZNDs together with other geodetic parameters. Due to data recording problems, the data on March 27th for all stations cannot be used. Three more days (March 20th, 21st and 22nd) for the Siu Lang Shui station and one more day (March 6th) for the Kau Yi Chau station also have similar problems. The ZNDs estimated for the six stations are given in Figure 7.

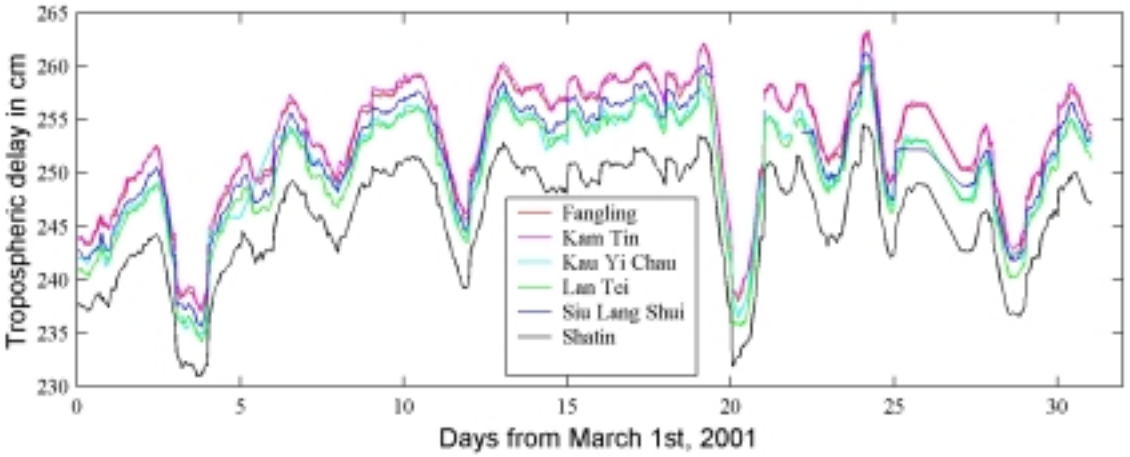

Figure 7. Hourly tropospheric ZNDs estimated for six GPS tracking stations

Since it is the differential atmospheric delays that affect the InSAR measurements (e.g., Rosen et al., 1996), we will look more closely at the differentiated ZNDs. The hourly ZNDs at each station are first differentiated with a time interval of one day and ten days, respectively. The results are then differentiated again between the stations. The histograms of the double differentiated ZNDs are given in Figure 8 (one-day interval) and Figure 9 (ten-day interval), respectively. A summary of the statistical results is given in Table 1.

Table 1 Statistics of double differentiated ZNDs

Interval	Max (cm)	Min (cm)	Mean (cm)	RMS (cm)
1 day	6.37	-5.18	0.016	1.077
10 days	6.12	-5.99	0.152	1.320

Although the peak-to-peak variability of the double differentiated ZNDs reach 11.55cm and 12.11cm respectively for the one-day and ten-day intervals (Table 1), Figures 8 and 9 show that the probability for such large values to occur is low. Under the assumption of Gaussian distribution, the double differentiated ZNDs for the results with a one-day interval range from –2.14cm to 2.17cm at the 95% significance level. The corresponding values for the results with a ten-day interval are –2.49cm and 2.79cm, respectively. Therefore the peak-to-peak variability of the results is 4.31cm and 5.28cm, respectively. When assuming a look angle of 23° (the look angle of the mid scene of the ERS-1/2 images), the ZNDs are translated into 9.36 cm and 11.47 cm of round trip radar signal delays. This level of tropospheric delays can make cm-level ground displacements unobservable and can introduce height errors as large as 320m and 390m for a perpendicular baseline of 100m.

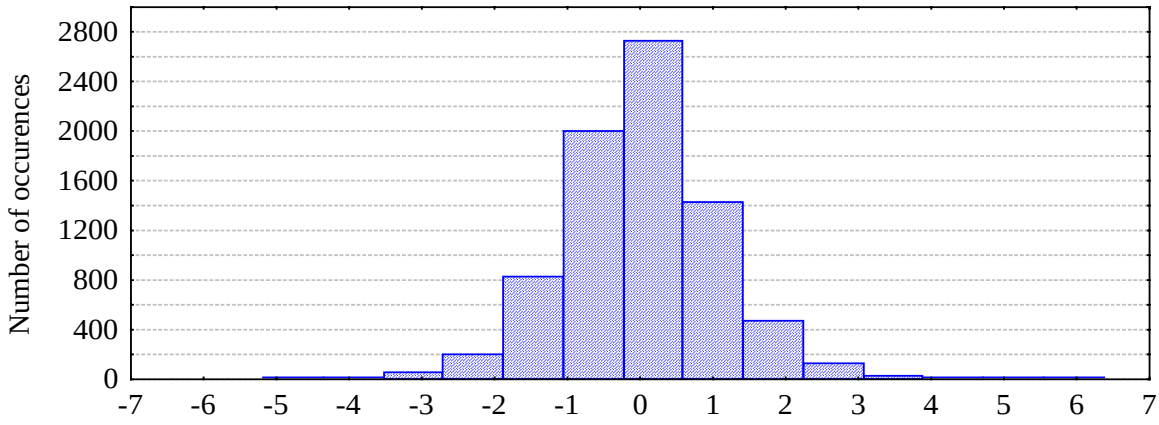

Figure 8. Histogram of double differentiated ZNDs (one-day interval)

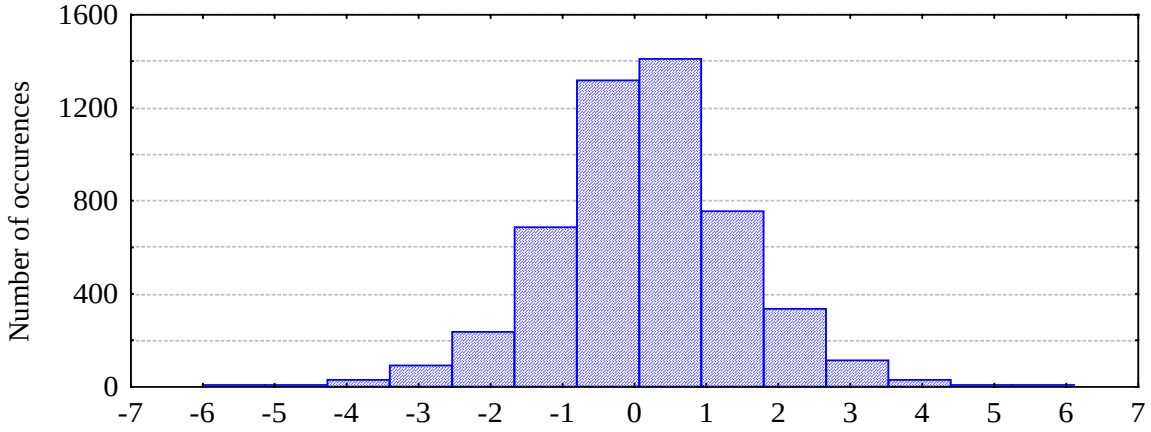

Figure 9. Histogram of double differentiated ZNDs (ten-day interval)

4. CONCLUSIONS

Atmospheric effects on InSAR measurements have been studied for the HK region based on an InSAR tandem image pair and a month-long GPS data obtained at five stations. The differential atmospheric delays determined from the SAR interferogram for two selected areas clearly follow the power law, consist with results obtained by other researchers. The respective RMS values of the differential atmospheric delays for the two areas are 2.12 rad and 3.40 rad, respectively.

The tropospheric ZNDs estimated from GPS measurements have shown significant temporal and spatial variations. They can potentially cause a peak-to-peak error of about 9.36 cm to a SAR interferogram at the 95% significance level for the one-day interval. The error increased to about 11.47 cm for the ten-day interval. This level of tropospheric delays can introduce dm errors to the measured ground displacements and a few hundred meters of errors to the measured terrain heights.

ACKNOWLEDGEMENTS

The first author is grateful to the Hong Kong Polytechnic university for the Postgraduate Research Scholarship provided. We thanks Dr. Yanxiong Liu for his help in processing the GPS data and for useful discussions.

REFERENCES

Bevis, M., Businger, S., Herring, T.A., Rocken, R., Anthes, R.A., and Ware, R.H. (1992), GPS Meteorology: Remote sensing of atmospheric water vapor using the Global Positioning System, *Journal of Geophysical Research*, 97(D14), p15787-15801.

Bock, Y. and Williams, S. (1997), Integrated Satellite Interferometry in Southern California, *EOS*, 78(29), p293, 299-300.

Ruf, C.S., and Beus, S.E. (1997), Retrieval of Tropospheric water vapor scale height from horizontal turbulence structure, *IEEE Trans. On Geoscience And Remote Sensing*, 35(2), 1997:203-211

Goldstein, R. (1995), Atmospheric limitations to repeat-track radar interferometry, *Geophysical Research Letter*, 22(18), p2517-2520.

Hanssen, R.F. (1998), Atmospheric heterogeneities in ERS tandem SAR interferometry, DEOS Report No.98.1, Delft University press, Delft, the Netherlands

Hanssen, R.F., Wechwerth, T.M., Zebker, H.A., and Klees, R. (1999), High-resolution water vapor mapping from interferometric radar measurements, *Science*, 283, p1297-1299

Massonnet, D., Feigl, K.L., Rossi, M. and Adragna, F. (1994), Radar interferometric mapping of deformation in the year after the Landers earthquake, *Nature*, 369, p227-230

Massonnet, D., and Feigl, K. L. (1995), Discrimination of geophysical phenomena in satellite radar interferograms, *Geophysical research letters*, 22(12), p1537-1540

Rosen, P.A., Hensley, S., Zebker, H.A. and et al. (1996), Surface deformation and coherence measurements of Kilauea Volcano, Hawaii, from SIR-C radar interferometry, *Journal of Geophysical Research*, 101(E10), p23109-23125.

Rosen, P.A., Hensley, S., Joughin, I.R. and et al. (1999), Synthetic Aperture Radar Interferometry, *Proceedings of The IEEE*, Vol. XX, No. Y.

Tarayre, H. and Massonnet, D. (1996), Atmospheric propagation heterogeneities revealed by ERS-1, *Geophysical Research letters*, 23(9), p989-992

Zebker, H. A., Rosen, P. A. and Hensley, S. (1997), Atmospheric effects in interferometric synthetic aperture radar surface deformation and topographic maps, *Journal of Geophysical Research*, 102(B4), p7547-7563.